21, rue d'Artois, F-75008 PARIS
http : //www.cigre.org

CIGRE US National Committee
2018 Grid of the Future Symposium

Using Computational Fluid Dynamics to Assess Dynamic Line Ratings in Southern Idaho

A.W. ABBOUD, J.P. GENTLE, T.R. MCJUNKIN, B.A. FEHRINGER, J.P. LEHMER
Idaho National Laboratory
USA

SUMMARY

The overall goal of the study is to combine computational fluid dynamics (CFD) simulations with weather data that is collected over a 1-year long period across southern Idaho to calculate the dynamic line ratings (DLR) of several transmission lines. These ratings can be compared to the static rating assumptions to show the potential for additional current carrying capacity along transmission lines through account for additional effects of convective cooling from the wind. The region of interest is quite large, sized at 144 km by 98 km; in order to cover this large region, the CFD simulations are split into four separate regions of over 80 million computational cells each. The weather data that was collected suggest initial assumptions used to make the static ratings were vastly over predicted with regards to summer temperatures and solar irradiance. The weather data is ran through the General Line Ampacity State Solver (GLASS) tool that was developed by Idaho National Laboratory (INL) to parse large quantities of weather data across thousands of transmission midpoint spans in the region. For shorter lines, the dynamic line ratings often show large improvement over static ratings. The case study here shows over 95% of the time DLR values are above static values on the short transmission lines. However, for long lines, a conundrum occurs, where due to the large number of weather stations associated with the line, there is often a single weather station which may read local wind speeds of zero. This often defaults the line rating to be limited by natural convective cooling and does not show as much improvement over static as might be expected from the weather data if DLR calculations are used with a minimum ampacity across all midpoints. Other methods with transient state calculations should be utilized for long lines.

KEYWORDS

Computational Fluid Dynamics; Dynamic Line Rating; Transmission Lines

alexander.abboud@inl.gov

INTRODUCTION

Line ratings are typically calculated as constant values using conservative assumptions for the weather conditions in the calculations. While there are some adjustments that are made on seasonal or daily basis, there is likely a lot of unused head room on overhead conductors. Dynamic Line Ratings (DLR) have been identified by the United States Department of Energy as a distribution infrastructure solution to defer upgrades, support line outages, and increase yields of distributed generation [1,2].

The line ratings based on maximum conductor temperatures have standard models developed by the International Council on Large Electric Systems (CIGRE) [3,4,5], the International Electrochemical Commission (IEC) [6], and the Institute of Electrical and Electronics Engineers (IEEE) [7,8]. The conductor maximum temperature limits the ampacity of a transmission lines to avoid sagging or clearance issue of the line segments between structures due to thermal expansion. The conservative nature of transmission line standards can be hard to adjust, so research showing the benefits of DLR is important to prove that the method is acceptable. Case studies utilizing weather data in the field has shown potential for DLR to increase ampacity above static throughout several countries [9,10,11,12,13].

This study utilizes the coupling of field weather data collected within the transmission corridor with Computational Fluid Dynamics (CFD) results. For the wind field simulations, the steady-state Reynolds-Averaged Navier Stokes (RANS) approach was used for turbulent modelling of the wind flow [14]. The RANS approach has been used to validate wind flows in complex terrains [15], with adequate speed up predictions [16], and low-elevation mountains within acceptable error [17,18]. Due to the convective cooling calculation, the error in the cooling rate scales as approximate the square root of the wind speed, so a 10% error in wind speed is only a 5% error in the cooling rate. The site of interest in southern Idaho is 144km by 98 km. This study first goes through the theory for CFD and DLR, then discusses the CFD results, weather data comparisons to static assumptions, and finally DLR comparisons to static ratings.

THEORY

Computational Fluid Dynamics

In order to run the CFD simulations, the domain of interest must be linearized, this is done through projection into the Idaho Transverse Mercator Projection [19]. The domain is then split into four different regions which cover the space. The elevation map is shown in Figure 1a, where the plain area is mostly in light brown and green, and the darker brown in the north are the mountains. The roughness map of the terrain is shown in Figure 1b, this shows regions of low to high vegetation and cities where near ground wind fields would be affected. These regions are not explicitly modelled in the CFD, so the roughness layer is used to approximate slowdowns due to these subgrid effects. The division of this terrain into four sectors for CFD analysis is shown in Figure 1c. Only the regions with large transmission lines are selected, and some sparsely populated regions are ignored (as these likely have zero or no congestion).

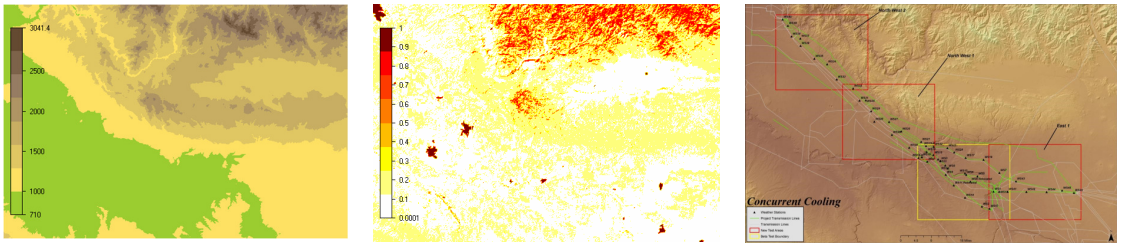

(a) (b) (c)

Figure 1. (a) The elevation map of the region, (b) the roughness map of the terrain, the division of the map into CFD domains around the transmission lines.

Each of the domains consists of 85 million computational cells, with 30-meter spatial resolution in the horizontal direction and varying spatial resolution vertically. The vertical resolution is spaced such that near the ground the resolution is in 5-meter increments to allow for accurate wind fields near the transmission lines, while above 100 meters a log scale is used up to the atmospheric boundary layer. For computing the wind speeds across the domain tiles the Wind Atlas methodology of Wind Sim is utilized [20].

The steady-state standard k-ε RANS model is used for modelling the turbulent kinetic energy and dissipation rate. The PDEs for the solution consist of the velocity vectors, the continuity equation, and equations for the turbulent kinetic energy and turbulent dissipation rates. The equation for the velocity vectors is

$$\rho U_i \frac{\partial U_j}{\partial x_i} = \frac{\partial}{\partial x_i}\left[(\mu + \mu_t)\left(\frac{\partial U_i}{\partial x_j} + \frac{\partial U_j}{\partial x_i}\right)\right] - \frac{\partial p}{\partial x_i} \tag{1}$$

The turbulent kinetic energy, k, equation is given by

$$\frac{\partial (U_i k)}{\partial x_i} = \frac{\partial}{\partial x_i}\left[\frac{\mu_t \partial k}{\sigma_k \partial x_i}\right] + P_k - \epsilon \tag{2}$$

And the equation for the turbulent dissipate rate, ϵ, is given by

$$\frac{\partial (U_i \epsilon)}{\partial x_i} = \frac{\partial}{\partial x_i}\left[\frac{\mu_t \partial \epsilon}{\sigma_\epsilon \partial x_i}\right] + c_{\epsilon 1}\frac{\epsilon}{k}P_k - c_{\epsilon 2}\frac{\epsilon^2}{k}P_k \tag{3}$$

Where the turbulent viscosity, μ_t is given by

$$\mu_t = \frac{C_\mu k^2}{\epsilon} \tag{4}$$

And the turbulent production term, P_k is given by

$$P_k = \mu_t\left(\frac{\partial U_i}{\partial x_j} + \frac{\partial U_j}{\partial x_i}\right)\frac{\partial U_i}{\partial x_j} \tag{5}$$

Where c_μ, c_{ϵ_1}, c_{ϵ_2}, σ_k, and σ_ϵ are the fixed constants for the $k-\epsilon$ model, with values set to 0.09, 1.55, 2.0, 1.0, and 1.3, respectively [14].

Dynamic Line Ratings

The dynamic ratings are calculated on 15-minute moving average intervals with 1-minute temporal resolution for the collected weather data. The heat balance equation is used to solve for the maximum current, *I*, to get [7]

$$I = \sqrt{\frac{q_c + q_r - q_s}{R(T_c)}} \tag{6}$$

Where q_c, q_r, and q_s are the convective, radiative and solar contributions, and *R* is the conductor resistance as a function of the conductor temperature T_c. The radiated heat loss per unit length in units of W/m is given by

$$q_r = 17.8D\epsilon\left[\left(\frac{T_c + 273.15}{100}\right)^4 - \left(\frac{T_a + 273.15}{100}\right)^4\right] \tag{7}$$

Where ϵ is the emissivity, T_a is the ambient air temperature and D is the conductor diameter. The heat gain through solar irradiance is given by

$$q_s = \alpha Q_{se} \sin(\theta) A' \tag{8}$$

Where α is the solar absorptivity, Q_{se} is the total solar and sky radiated heat flux corrected by elevation, θ is the effective angle of incidence of the sun's rays and A' is the projected area of the conductor. The convective heat loss is calculated using one of three equations for high wind speeds, low wind speed (below 3 mph) or natural convective cooling. For high wind speed the equation is given by

$$q_{c1} = \left[1.01 + 1.35\left(\frac{DV_w\rho_f}{\mu_f}\right)^{0.52}\right] k_f K_{angle}(T_c - T_a) \tag{9}$$

For low wind speed the equation is given by

$$q_{c2} = 0.754\left(\frac{DV_w\rho_f}{\mu_f}\right)^{0.6} k_f K_{angle}(T_c - T_a) \tag{10}$$

Or for natural convection the equation is given by

$$q_{cn} = 3.645\rho_f^{0.5} D^{0.75}(T_c - T_a)^{1.25} \tag{11}$$

Where V_w is the speed of air, with fluid parameters density ρ_f, viscosity μ_f and thermal conductivity k_f calculated at the ambient temperature. And K_{angle} is the wind direction factor which can vary from about 0.3 to 1.0 based on parallel or perpendicular wind flow to the transmission line, given by

$$K_{angle} = 1.194 - \cos(\phi) + 0.194\cos(2\phi) + 0.368\sin(2\phi) \tag{12}$$

Where ϕ is the angle of incidence between the wind and the transmission line midpoint. The GLASS code developed by INL does all of these calculations for every single transmission line midpoint of interest. The minimum value among all the midpoint calculations is assumed to be the ampacity for each line.

RESULTS

Computational Fluid Dynamics

The results for the wind fields are shown in Figure 2 for each of the four domain decompositions. This is shown for both the north incoming and the south incoming sector. The direction of the incoming wind will impact where slower near-ground wind speeds occur. The northwest-1 and -2 sectors are closer to the large mountain ranges and show significant changes in speed compared with the case when wind comes from the north.

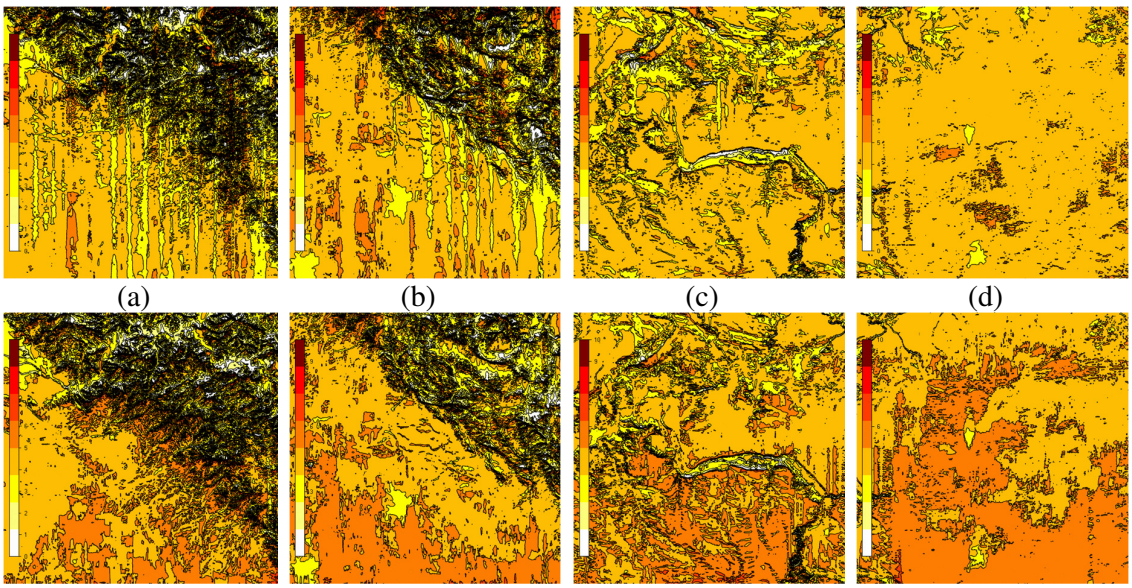

Figure 2. Wind field flow for the northwest-2, northwest-1, center, and east domain sections for north incoming (a-d) and south incoming wind (e-h), respectively. The color bar is scaled from 0 to 10 m/s.

Weather Data

A summary of one of the weather stations is shown, with comparison to the static assumptions. This weather station is located at the north-western portion of the terrain. Histograms for speed, temperature, and solar are shown in Figure 3a, 3b, and 3c, respectively. The difference from static as a percentage of time over the year is shown in Figures 3d, 3e and 3f for those same variables.

For this particular weather station, the wind speed is greater than the static assumption 63% of the time. This rating has both winter and summer seasonal adjustments on temperature and solar. For the ambient temperature, the values were below static 99% of the time in the summer, and below static 47% of the time in the winter. For the solar irradiance, the values were less than static assumptions 100% of the time in summer, and 95% of the time in winter. Trends are similar for the other 46 weather stations placed throughout the region.

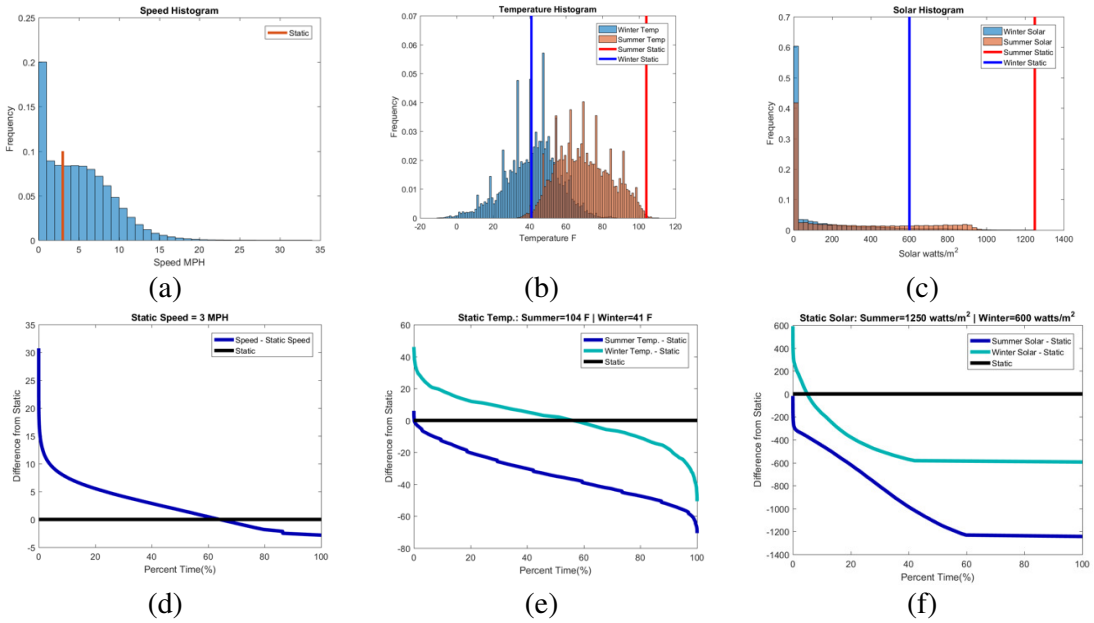

Figure 3. Example of weather data in the region, (a) histogram of wind speed, (b) histogram of temperature, (c) histogram of solar irradiance, and percentage of time above static for (d) wind speed (e) temperature and (f) solar irradiance.

Transferred Climatology

Example transfers are shown from the weather station to different midpoint spans using the wind fields from the CFD model. This transferred data gives updated wind speeds to use at the transmission line locations for the ampacity rating. Figure 4 shows how the data is processed though the CFD fields to different midpoint locations. The right side of this plot shows the wind data collected at three different weather station locations, while the left side shows the corresponding transferred wind rose after the CFD lookup table has been applied to each incoming wind direction. These wind roses show the frequency of both the wind speed and wind direction in the region. For flat regions of the terrain, the transferred wind rose may change only slightly – such as in the first row of transfers this weather station and midpoints are in a flat region of the terrain. While for hilly regions, the max wind speeds, and predominate wind directions can change the values, as shown in the second row in Figure 4. Nearby hills may block or redirect the wind incoming from the western and north-western directions when comparing locations along the foothills.

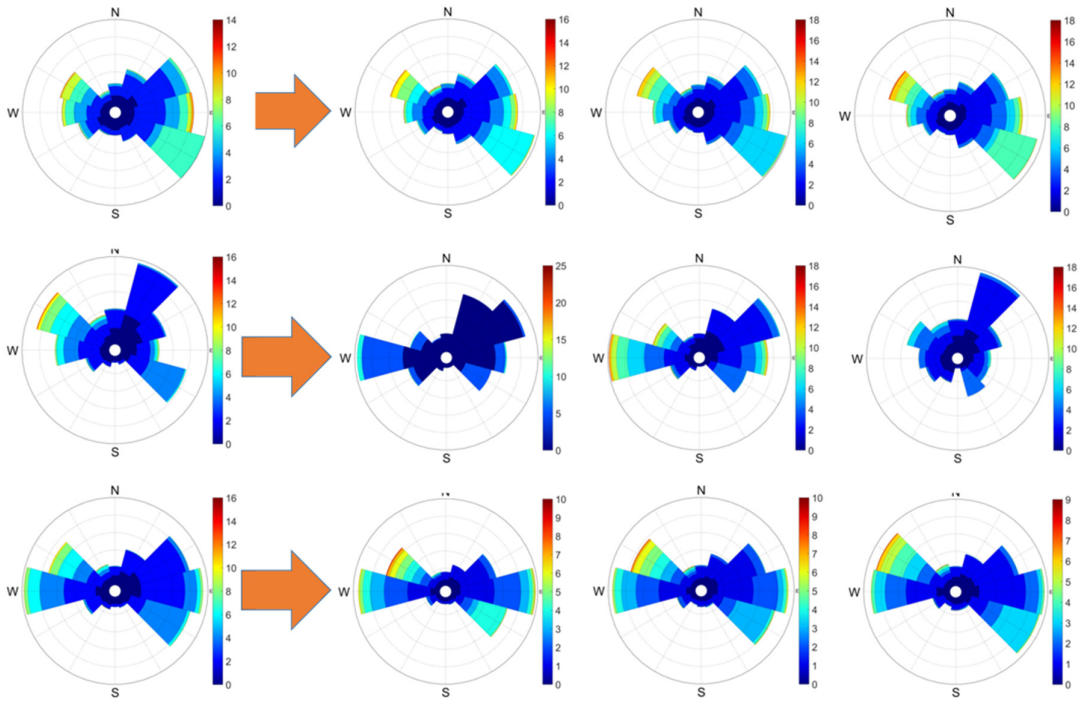

Figure 4. Example of transferred weather conditions of wind speed and direction based on the CFD lookup tables. These are wind roses that show the combined frequency of the wind speed and wind direction.

DLR Calculations

The dynamic line ratings are calculated for every major transmission line in the region using the GLASS code. For short lines with few weather stations, significant improvements are shown. In Figure 5a the 15-minute moving average of the ampacity for a short line of 3.1 miles with a small conductor with 2 weather stations is shown, with the summer and winter ratings shown with dotted overlay. Figure 5b shows the amount of time the rating is above static, in the winter the DLR rating is above the static rating nearly 80% of the time, and the DLR is above the summer rating is about 95% of the time. From Figure 3a and 3b, this is likely that due to low wind speeds below static assumption occurring some of the time, as well as the winter temperature assumption as more of an average rather a conservative value such as in the summer. In Figure 5c the 15-minute average for a large conductor line is shown which is only 1 mile long with 2 nearby weather stations. For this line the DLR calculated above static is shown in Figure 5d, where the time above the winter rating is about 60%, and the time DLR is above the summer static rating is about 95%.

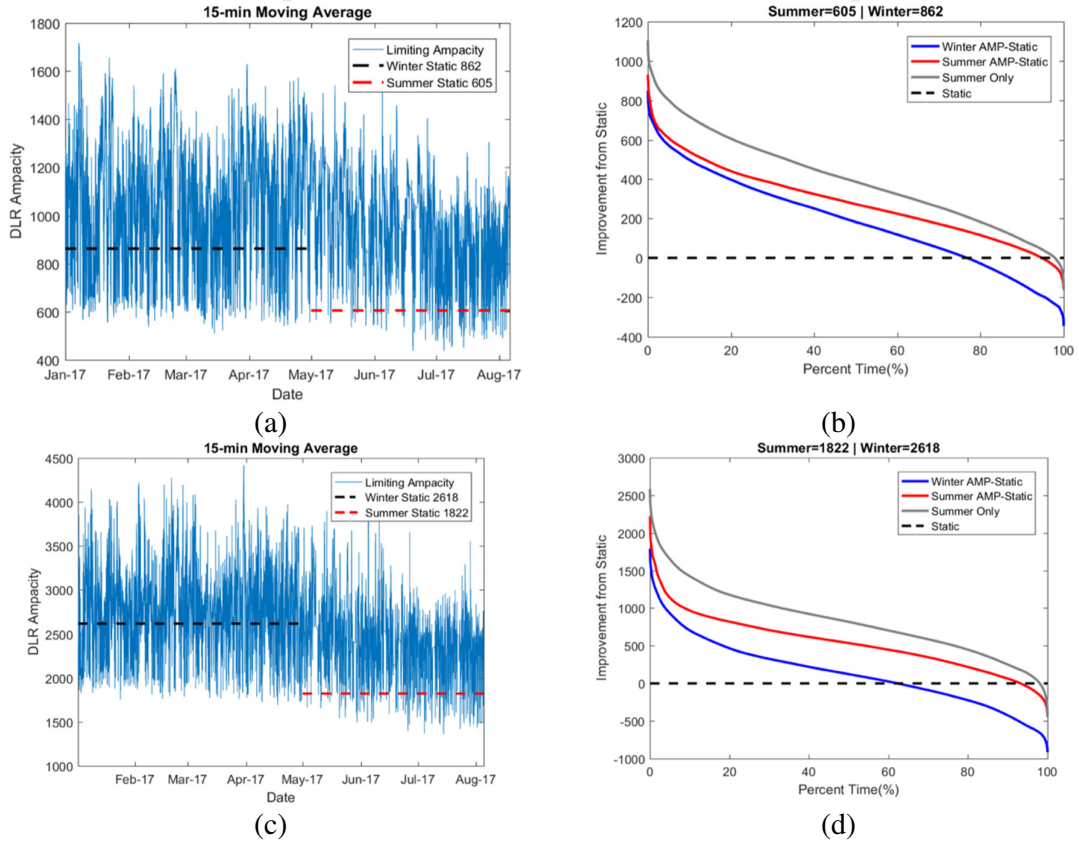

Figure 5. The 15-minute moving average ampacity calculations for a (a) small conductor and (c) large conductor in the Boise-Twin Falls regions compared to static ratings, (c) small conductor DLR time above static and (d) large conductor DLR time above static rating.

For longer transmission lines, care needs to be taken in the applications of the DLR calculation. A large conductor which spans the entire region, of about 100 miles in length with 30 weather stations used for its DLR calculation has its 15-minute moving average of the ampacity plotted in Figure 6a. In the winter, the DLR ampacity is well below the static rating compared to the previous lines shown. The percentage of time above static plot for this long line is shown in Figure 6b, for this during the winter the DLR value is only above static 5% of the time, and for the summer, it is only 55% of the time.

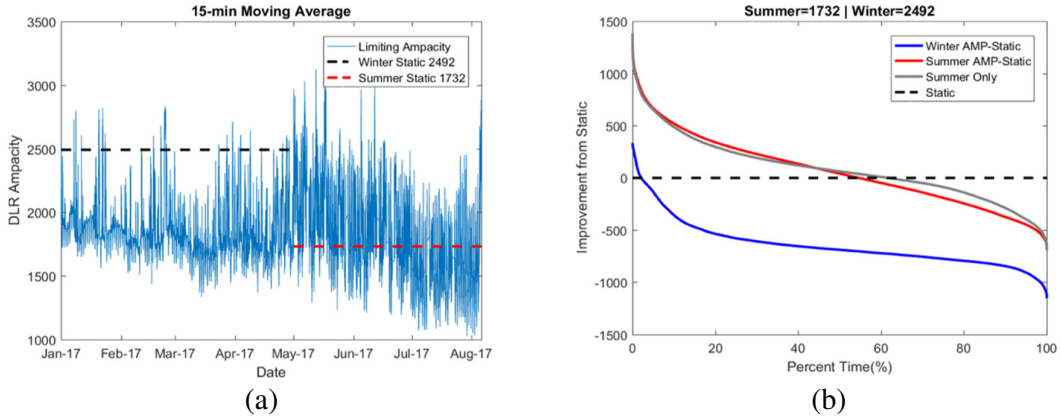

Figure 6. The (a) 15-minute moving average for a large conductor of about 100 miles with 30 weather stations, and (b) the conductor time DLR is above the static rating.

In Figure 7a, the weather speed for all 30 weather stations associated with this long line are shown for a single day, along with the minimum at each timestamp. Figure 7b shows the wind speed histogram of a single station, where it seems as if the wind speeds should be on the higher side contributing much to the convective cooling effect. Figure 7c shows the histogram of the minimum wind speed (the black line in Figure 7a), which shows about 80% of the time the wind speed at one of the weather stations is near 0. For long lines with many weather stations, then the sheer number of values can cause a single weather station to show zero wind speed, which limits the DLR to natural convective cooling only. Utilizing DLR directly in this case would still benefit from solar irradiance and ambient temperature differences, but these are small compared to the wind speeds. Consider that, in general, weather stations in the region may read a near-zero value in the wind speed 5% of the time such that the cooling is driven by natural convection, then the probability that a line with 30 weather stations on it all reading not zero values would be $P(>0) = 0.95^{30}$ (ignoring correlated effects). From this quick calculation, over the yearlong span of data, only 20% of the time all 30 weather stations read a non-zero value. This means that in the DLR calculation, 20% of the time will default to natural convective cooling. However, it should be noted that for a line this long, changes in the ampacity could be reflected with a transient state calculation. Due to large-scale temperature and wind changes, not every midpoint span would be at the same conductor temperature. Other algorithms with transient state calculations such as autoregressive–moving-average or true dynamic line rating should be considered for the DLR calculations for long transmission lines.

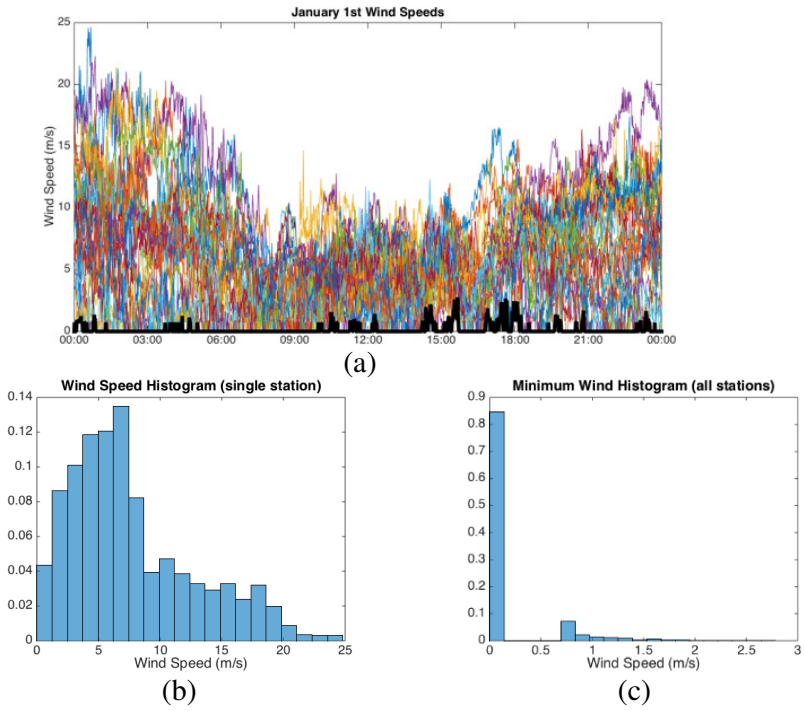

Figure 7. (a) The wind speed over a day long region for all the weather stations along the line, and the minimum speed of these 30 weather stations shown in the thick black line, (b)

the histogram for a single weather station, and (c) the histogram for the minimum speed of all the weather stations.

CONCLUSION

Transmission corridor collected field weather data can be coupled with computational fluid dynamics results to calculate local DLR for every midpoint span along a transmission line. The GLASS software developed by INL was used to process the large amount of historical information gathered in a yearlong span to calculate dynamic line ratings for several transmission lines. The field data alone showed that for this particular region's summer temperature assumptions and solar irradiance assumptions used in static ratings are often too conservative. For short transmission lines, the benefit of DLR was shown to be quite large during summer when more congestion would be expected from HVAC load, the DLR value is above static ratings about 95% of the time in the summer.

For the long line that was analyzed, the raw value of the ampacity was not as generous towards the benefits of DLR. However, in actuality the entire 100-mile transmission line would not be expected to be at the same conductor temperature at every midpoint span due to different convective cooling rates – which was an assumption made in these DLR calculations. In the future, improved algorithms such as autoregressive–moving-average (ARMA) may be utilized for calculations for each midpoint and may alleviate the many weather station long line conundrum. Other methods for improving this issue have been hypothesized such as true dynamic line rating with individual temperature estimates, which will be examined in future studies.

ACKNOWLEDGEMENTS

This research was performed by Idaho National Laboratory with support from Idaho Power Company and funding from the U.S. Department of Energy Wind Energy Technologies Office. INL is operated by Battelle Energy Alliance under contract No. DE-AC07-05ID14517.

BIBLIOGRAPHY

[1] "Dynamic line rating systems for transmission lines: American recovery and reinvestment act of 2009," U.S. Department of Energy, Tech. Rep., 2014.
[2] "Smart grid system report," U.S. Department of Energy, Tech. Rep., 2010.
[3] CIGRE Working Group 22.12, "The thermal behaviour of overhead line conductors," Electra, vol. 114, no. 3, pp. 107–125, 1992.
[4] "Guide for selection of weather parameters for bare overhead conductor ratings," CIGRE WG 22.12, Tech. Rep., 2006.
[5] "Guide for thermal rating calculations of overhead lines," CIGRE WG B2.43, Tech. Rep., 2014.
[6] "Overhead electrical conductors calculation methods for stranded bare conductors," IEC Standard TR 1597, Tech. Rep., 1985.
[7] "Standard for calculating current-temperature relationship of bare overhead line conductors," IEEE Standard 738, Tech. Rep., 2012.
[8] IEEE PES WG Subcommittee 15.11, "Real-time over- head transmission line monitoring for dynamic rating," IEEE Transactions on Power Delivery, vol. 31, no. 3, 2016.

[9] D. Greenwood, J. Gentle, K. Myers, P. Davison, I. West, J. Bush, G. Ingram, and M. Troffaes, "A comparison of real-time thermal rating systems in the U.S. and the U.K." IEEE Trans. Power Delivery, vol. 29, no. 4, pp. 1849– 1858, August 2014.
[10] B. P. Bhattarai, J. P. Gentle, P. Hill, T. McJunkin, K. S. Myers, A. Abboud, R. Renwick, and D. Hengst, "Trans- mission line ampacity improvements of altalink wind plant overhead tie-lines using weather-based dynamic line ratings," in IEEE PES General Meeting, July 2017.
[11] B. P. Bhattarai, J. P. Gentle, T. McJunkin, P. J. Hill, K. Myers, A. Abboud, and D. Hengst, "Improvement of transmission line ampacity utilization by weather-based dynamic line ratings," IEEE Transactions on Power De- livery, 33(4), pp 1853-1863.
[12] S. Uski-Joutsenvuo and R. Pasonen, "Maximizing power line transmission capability by employing dynamic line ratings technical survey and applicability in finland, vtt- r-01604-13," Tech. Rep., 2013.
[13] B. J. L. Aznarte and N. Siebert, "Dynamic line rating using numerical weather predictions and machine learning: A case study," IEEE Trans. Power Delivery, vol. 32, no. 1, pp. 335–343, 2017.
[14] W. Jones and B. Launder, "The prediction of laminarization with a two-equation model of turbulence," International journal of heat and mass transfer, vol. 15, no. 2, pp. 301–314, 1972.
[15] T. Wallbank, "Windsim validation study: Cfd validation in complex terrain," Tech. Rep., 2008. [Online]. Available: http://www.windsim.com/documentation/paperspresentations/thesis/080512trw%20WindSim%20Write% 20Up%20-%20Validation%20study.pdf
[16] A. Dhunny, M. Loolchund, and S. Rughooputh, "Numerical analysis of wind flow patterns over complex hilly terrains: comparison between two commonly used cfd software," International Journal of Global Energy Issues, vol. 39, no. 3, pp. 181–203, 2016.
[17] A. Dhunny, M. Loolchund, and S. Rughooputh, "A high-resolution mapping of wind energy potentials for mauritus using computational fluid dynamics," Wind and Structures, vol. 20, no. 4, pp. 565–578, 2015.
[18] A. Dhunny, M. Loolchund, and S. Rughooputh, "Wind energy evaluation for a highly complex terrain using computational fluid dynamics (cfd)," Renewable Energy, vol. 101, pp. 1–9, 2017.
[19] Idaho Department of Water Resources. Idaho Transverse Mercator Projection. https://www.idwr.idaho.gov/GIS/IDTM/
[20] S. Koller and T. Humar, "Windpotentialanalyse fur windatlas jaresmittelwete der modellierten windgeschwindigkeit," Energieschweiz, Bern, Switzerland, Tech. Rep., 2016. [Online]. Avail- able: http://www.bfe.admin.ch/geoinformation/05061/06675/index.html?lang=en&dossier id=06606